

Universal decay cascade model for dynamic quantum dot initialization

Vyacheslavs Kashcheyevs^{1,2} and Bernd Kaestner³

¹*Faculty of Computing, University of Latvia, Riga LV-1586, Latvia*

²*Faculty of Physics and Mathematics, University of Latvia, Riga LV-1002, Latvia*

³*Physikalisch-Technische Bundesanstalt, Bundesallee 100, 38116 Braunschweig, Germany*

Dynamic quantum dots can be formed by time-dependent electrostatic potentials in nanoelectronic devices, such as gate- or surface-acoustic-wave-driven electron pumps. Ability to control the number of captured electrons with high precision is required for applications in fundamental metrology and quantum information processing. In this work we propose and quantify a scheme to initialize quantum dots with a controllable number of electrons. It is based on the stochastic decrease in the electron number of a shrinking dynamic quantum dot and is described by a nuclear decay cascade model with “isotopes” being different charge states of the dot. Unlike the natural nuclei, the artificial confinement is time-dependent and tunable, so the probability distribution for the final “stable isotopes” depends on the external gate voltage. We derive an explicit fitting formula to extract the sequence of decay rate ratios from the measurements of averaged current in a periodically driven device. This provides a device-specific fingerprint which allows to compare different devices and architectures, and predict the upper limits of initialization accuracy from low precision measurements.

PACS numbers: 73.63.Kv, 73.23.Hk, 73.21.La, 73.22.Dj

Single electron charging effects have attracted much interest since the proposal of single electronics [1] and the possibility to fabricate nanoscale structures. In particular, quantum dots (QD) connected to leads have been a standard model system for many years to study single charges in so called artificial atoms. Dynamic QDs, which are repeatedly formed and manipulated by time-varying confining potentials appear in particular in structures proposed to study quantum information [2–7]. One of the issues to be addressed is the decoupling of the QD from the environment and at the same time allowing the fast initialization with a controllable number of electrons. A suitable method has been demonstrated by Kataoka *et al.* [6] which uses pulses of surface acoustic waves (SAWs) to populate or depopulate a QD that is well isolated from electron reservoirs. While this mechanism is not yet fully understood, a more conventional approach [8] is adiabatic decoupling of the QD from electron reservoir, keeping the voltage on the QD fixed in a Coulomb blockade valley separating the discrete charge states. This strategy is limited by (i) non-adiabatic excitation of the QD [9] due to necessary finite decoupling rate, and (ii) experimental difficulties in tuning the lead-dot coupling to zero without disturbing the electrostatic potential on the QD, φ .

Here we propose and quantify an alternative scheme to achieve initialization by allowing non-equilibrium relaxation (backtunneling) from a QD being raised energetically above the Fermi level during the decoupling process. This process is known to play a role in several types of non-adiabatic current generation devices [10–14]. We identify scale separation in integrated time-dependent electron escape rates between the subsequent charge states as a precondition for low-dispersion initialization. In our decay-cascade model a voltage parameter

V shifts the hierarchy of the decay rates and thereby tunes the target number of electrons, n_0 , and the corresponding error $\langle (n - n_0)^2 \rangle$. The minimal error is then given by the particular QD implementation and fixed, for instance, by QD geometry. We proceed to analyze the results of recent non-adiabatic current generation experiments [15–17] and find them to be promising realizations of the proposed initialization scheme. Based on the decay cascade model predictions we propose an indirect way to measure the initialization accuracy in these devices by extracting the decay rate hierarchy fingerprint from low precision measurements of their current-voltage characteristics. Finally, possible strategies for accuracy improvement are discussed based on the ways charging energy, temperature and barrier design affect the electron escape rates.

Decay cascade model. The initialization process is shown pictorially in Fig. 1a. The relaxation rate of electrons in the QD, $\Gamma_{RC} = (RC)^{-1}$, is reduced at a characteristic speed $\beta = |\dot{\Gamma}_{RC}/\Gamma_{RC}|$. (Here R and C are the resistance and the capacitance of the QD with respect to its environment, respectively.) Simultaneously, $\varphi(t)$ grows more negative. Ejection of electrons at rate $\Gamma_{ad} = |e\dot{\varphi}/E_c|$ is required for the electron number distribution $P_n(t)$ to stay close to instantaneous equilibrium ($E_c = e^2/C$ is the charging energy and e is the electron charge). Such adiabatic following becomes impossible due to insufficient escape rate at times beyond the non-adiabatic crossover time t_0 defined by $\Gamma_{RC}(t_0) = \Gamma_{ad}$. Crucially for our scheme, if Γ_{ad} can be made much larger than β then excitation from the Fermi sea [9] can be ignored while the QD remains loose enough at $t > t_0$ to “forget” the adiabatic initial condition $P_n(t_0)$ and yield eventual accuracy dictated by the decay cascade mechanism.

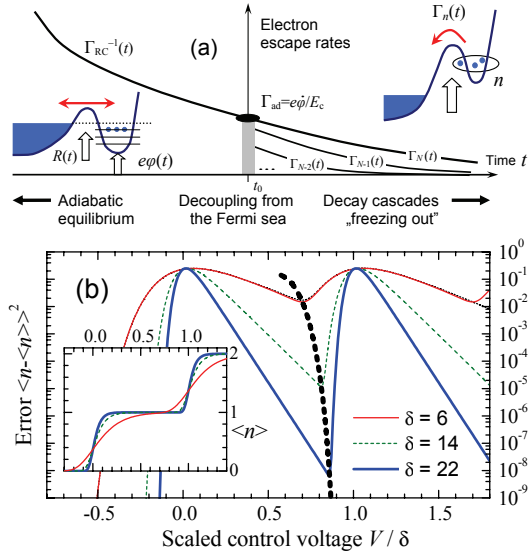


FIG. 1. (color online) (a) Overview of the model. (b) Main results: the variance, $\langle n - \langle n \rangle \rangle^2$, and the average (inset), $\langle n \rangle$, of the number of captured electrons n , for $\alpha_n = 1$, $\delta_1 = 0$ and $\delta_n = \delta$ as functions of control voltage V (in units of δ). All results are calculated using $N = 5$ and Eq. (4), except for the thin dotted line that shows Eq. (10) with $N = 2$. The thick dotted line traces the position and the value of variance as δ is varied.

For $t > t_0$ we write down a general kinetic equation

$$dP_n(t)/dt = -\Gamma_n(t) P_n(t) + \Gamma_{n+1}(t) P_{n+1}(t), \quad (1)$$

$$P_n(t_0) = \delta_{n,N}, \quad \lim_{t \rightarrow \infty} \Gamma_n(t) = 0, \quad (2)$$

where Γ_n is the decay rate of the charge state with n electrons on the QD. The empty dot ($n = 0$) is an absorbing state, $\Gamma_0 \equiv 0$, and the distribution is normalized, $\sum_{n=0}^{\infty} P_n = 1$. N is the initial number of electrons and $\Gamma_N(t_0)$ is identified with Γ_{ad} (see Fig. 1a). The use of Eqs. (1)–(2) to describe QD initialization assumes (i) randomization of the microstate corresponding to a given n on a time scale $\tau \ll \Gamma_n^{-1}$ so that Markov approximation is justified and the transition rates Γ_n are well-defined, (ii) no additional loading of electrons into the QD after t_0 , and (iii) sharp initial condition, Eq. (2) (the latter is non-essential). The system of equations (1) is rather general, and has also been used in the context of dynamic QD evolution [13, 18] (although not for the initialization stage).

A general iterative solution to Eq. (1) is

$$P_n(t) = \int_{t_0}^t e^{-\int_{t'}^t \Gamma_n(\tau) d\tau} \Gamma_{n+1}(t') P_{n+1}(t') dt', \quad (3)$$

where $P_{N+1}(t) = \delta(t - t_0)/\Gamma_{N+1}(t_0)$ ensures fulfillment of the initial condition (2). Our strategy is, firstly, to identify the general properties of Eq. (3) that result in a well-defined final electron number, and, secondly, to in-

troduce more specific physical assumptions that connect the model with potential experimental realizations.

Conditions for accurate initialization. Consider an additional assumption (which can be relaxed later) that time-dependence of $\Gamma_n(t)$ is the same for all n , namely, $\Gamma_n(t)/\Gamma_{n-1}(t) \equiv e^{\delta_n} = \text{const}$. In this case the final ($t \rightarrow \infty$) distribution P_n depends only on the dimensionless integrals $X_n \equiv \int_{t_0}^{\infty} \Gamma_n(t) dt$ and is given by

$$P_n(\infty) = \sum_{k=n}^N Q_{nk} C_k e^{-X_k}, \quad (4)$$

$$C_k = -\sum_{m=k+1}^N C_m Q_{km}; \quad C_N = 1, \quad (5)$$

$$Q_{nk} = \prod_{m=n}^{k-1} \frac{X_{m+1}}{X_m - X_k}; \quad Q_{nn} = 1. \quad (6)$$

The solution (4) is rather unilluminating, but can be investigated numerically (see below). For now let us focus on the limit of cascade timescale separation:

$$\dots \gg X_{n+1} \gg X_n \gg X_{n-1} \gg \dots \quad (7)$$

In this limit Eq. (6) simplifies to $Q_{k-1,k} = -1$ and $Q_{nk} = 0$ for all $n < k - 1$. This in turn means that $C_n = 1$ for all $0 \leq n \leq N$. The solution becomes $P_N(\infty) = e^{-X_N}$ and

$$P_n(\infty) = e^{-X_n} - e^{-X_{n+1}} \quad \text{for } 0 < n < N. \quad (8)$$

Our model is justified for $\Gamma_N(t_0) \gg |\dot{\Gamma}_N/\Gamma_N|$, which implies $X_N \gg 1$ (for smoothly decaying rates). Thus there will be such integer $n_0 < N$ that

$$X_{n_0+1} > 1 > X_{n_0} \quad \text{and} \quad X_{n_0+1} \gg X_{n_0}. \quad (9)$$

Under Eq. (7) it is sufficient to consider only three probabilities to be non-zero:

$$\{P_{n_0+1}, P_{n_0}, P_{n_0-1}\} = \{e^{-X_{n_0+1}}, e^{-X_{n_0}} - e^{-X_{n_0+1}}, 1 - e^{-X_{n_0}}\}. \quad (10)$$

We see that the probability distribution is dominated by $P_{n_0} \rightarrow 1$ if $X_{n_0+1} \gg 1$ and $X_{n_0} \ll 1$. The meaning of this condition is simple: the state with $n_0 + 1$ electrons is unstable enough to have decayed while n_0 is stable

Time-scale separation expressed by Eq. (7) can be taken into account directly in the most general solution (3), without requiring same time-dependence of $\Gamma_n(t)$'s. The mathematics of this derivation can be summarized as follows: (a) observe that $\Gamma_{n+1} P_{n+1} = -\frac{d}{dt} \sum_{m>n} P_m$ exactly; (b) assume that all $P_m(t)$'s with $m > n$ compared to $P_n(t)$ itself vary on a time-scale much closer to t_0 , so that $\Gamma_{n+1}(t') P_{n+1}(t') \propto \delta(t_0 - t')$ in Eq. (3); (c) solve the resulting $P_n(\infty) = e^{-X_n} (1 - \sum_{m=n+1}^N P_m)$ to get

$$P_n(\infty) = e^{-X_n} \prod_{m=n+1}^N (1 - e^{-X_m}). \quad (11)$$

Finally, examining Eq.(11) under condition (9) reveals difference from Eq. (10) of at most X_{n_0} which is reached at $X_{n_0} \ll X_{n_0+1} \approx 1$.

Parametric control of decay rate hierarchy. Usefulness of Eq. (4) is limited unless dependence of X_n 's on commonly accessible external control parameters can be established. Typically, escape rates depend exponentially on the height of the confining barrier, which in turn can be controlled by a gate voltage V . Tuning the decay rates $\Gamma_n(t)$ by V would affect all decay rates simultaneously. Thus we propose

$$\ln X_n = -\alpha_n V + \sum_{i=1}^n \delta_i. \quad (12)$$

Here α_n and δ_n are phenomenological constants that can be readily extracted experimentally as discussed below.

Figure 1b shows the behavior of the first two moments for equal and fixed $\alpha_n = 1$ and $\delta_n = \delta$ ($\delta_1 = 0$ is a mere shift of V). For $\delta > 6$ the difference between the approximations (4), (10) and (11) is negligible and Eq. (10) is sufficient to describe the n_0 -th step of a staircase $\langle n \rangle(V)$ regardless of N . The minimal variance $\langle n - \langle n \rangle \rangle^2$ is achieved at optimal values of V that are easily found from Eqs. (10) and (12). The minimal value of $1 - P_1(V)$ decays roughly exponentially with δ .

Possible experimental realizations. We expect to find good candidates for experimental realization of the proposed initialization mechanism among dynamic-QD-based electron pumps since backtunneling relaxation has been found [10, 14] to take place during certain parts of the pump cycle. The pumped current I_{pump} consists of electrons captured from the source and subsequently ejected into the drain. It can be related to model prediction via

$$I_{\text{pump}} = ef \langle n \rangle \equiv ef \sum_n n P_n(\infty) \quad (13)$$

(f is the frequency which the pump cycle is repeated) provided that (a) ejection to the drain starts after the escape back to the source has stopped, and (b) the ejection is complete. In some experimental settings there is strong evidence that the latter condition can be ensured [13, 19] while in others [10, 11] conditions (a) and (b) have been conjectured based on electrostatic modeling.

We have used the ansatz (12) and the solution (4) in Eq. (13) to fit experimental data from various electron pump devices [15–17], the results are shown in Fig. 2. In all cases α_n were found to vary weakly with n , so we have set $\alpha_n = \alpha$ constant for the entire voltage range for each device. Data set “a” in Fig. 2 was obtained in Ref. 15 for a silicon nanowire metal-oxide-semiconductor field-effect transistor (FET) driven by voltage pulses, while the data labelled “b” correspond to a sinusoidal modulation of an AlGaAs/GaAs nanowire metal-semiconductor FET in the quantum Hall regime [16]. Yet another realization is exemplified by the data obtained in Ref. 17, for an AlGaAs/GaAs split-gate device (“c” in Fig. 2), where the time dependent potential was generated by SAWs. The voltage applied to the split gate superimposes the SAW-

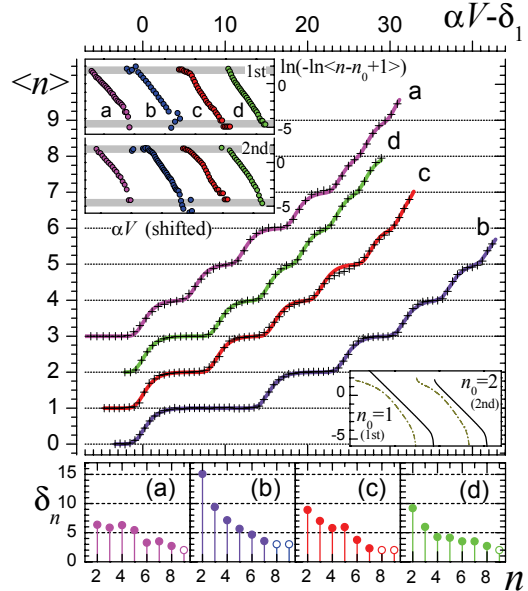


FIG. 2. (color online) Upper panel, main graph: decay cascade model fits (solid line) compared to measured current $I/(ef)$ (pluses) from Fig. 2a of Ref. 15 (a, magenta), Fig. 1a of Ref. 16 (b, blue), and Fig. 1 of Ref. 17 (c, red), and to classical simulation results from Fig. 6 of Ref. 11 (d, green). The graphs are shifted vertically for clarity. Insets are discussed in the text. Lower panels: fitted values of δ_n for each case.

potential and tunes the height of the confining barriers corresponding to the control voltage V .

Figure 2 demonstrates particular advantage of $\alpha_n = \alpha$: ($n-1$)-th step in $I_{\text{pump}}(V)$ has the length of δ_n on the scale of $\alpha V - \delta_1$. Thus the set of voltage-independent $\delta_n = \ln X_n / X_{n-1}$ can be used as a fingerprint of a particular device, see the lower panels in Fig. 2. Plotting $\ln(-\ln \langle n - n_0 + 1 \rangle)$ as a function of V serves as a quick test of the ansatz (12) since the plateaux part dominated by X_{n_0} must show up as a straight line. This is demonstrated in the lower right inset of Fig. 2 for the analytic $\langle n \rangle$ with $\delta = 6$ (same parameters as in Fig. 1b) and in the upper left inset for the empirical data (same data sets as in the main panel). For contrast, we show by a green dash-dotted line an *ad hoc* fit with a sum of symmetric Fermi-like step functions; the deviation from the cascade model is notable.

Our results for the second moment can be tested by measuring the low-frequency shot noise power spectral density [20]

$$S = 2e^2 f (\langle n^2 \rangle - \langle n \rangle^2). \quad (14)$$

Beyond the conditions (a) and (b) discussed above, Eq. (14) assumes [20] that (c) the temporal width $d\tau$ of the electron ejection current pulse is much less than the repetition period, $d\tau f \ll 1$. This regime has been probed experimentally by Robinson and Talyanskii [21], and we find good agreement with their data, see Fig. 3.

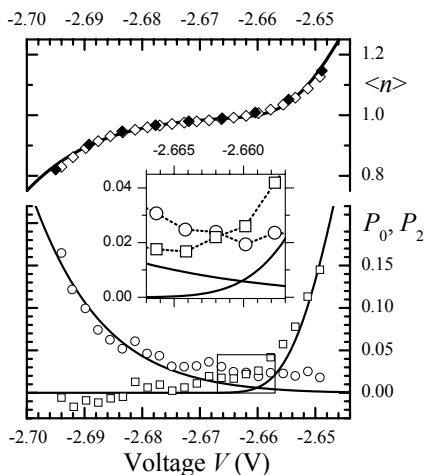


FIG. 3. Comparison to shot noise measurements on a SAW pump taken from Fig. 4a of Ref. 21. Upper panel: measured $I_{\text{pump}}/(ef)$ [\blacklozenge from $I_{\text{pump}}(V)$, \diamond from $P_0(V)$ and $P_2(V)$] and calculated $\langle n \rangle$ (solid line). Parameters fitted in Eq. (4) with $N = 2$ and $\alpha_1 = \alpha_2$: $\alpha_1 = 92.04 \text{ V}^{-1}$, $\delta_1 = -240.7$ and $\delta_2 = 6.252$. Lower panel and central inset: experimental probabilities P_0 (\circ) and P_2 (\square) compared to Eq. (4) (solid line) with parameters derived from the fit to I_{pump} .

Discussion and outlook. From the observations demonstrated in Figs. 2 and 3 we conclude that the decay cascade initialization scheme can be readily implemented experimentally. Several ways of controlling δ_n , thus achieving more accurate initialization can be suggested: (a) tighter confinement to increase the charging energy, (b) employing more energy-selective barriers [22], or (c) lowering the local temperature. Suggestion (c) applies when escape is determined by thermal activation. Note that this classical regime was investigated in electron dynamics simulations of Robinson and Barnes [11], see trace “d” in Fig. 2, which demonstrates the universality of the decay-cascade model. Within a classical independent electron picture, δ_n would be controlled by the difference in barrier height for the most energetic electron, $\delta_n \approx a(E_n - E_{n-1})$ where E_n is the ionization energy of a QD with n electrons, and a is an inverse effective temperature in this picture. The experiment of Ref. 15 may have operated under these conditions since the reported temperature $T = 20 \text{ K}$ is relatively high. The value of $\delta_2 = 6.4$ from Fig. 2 then gives $E_C = 11 \text{ meV}$ in agreement the experimental estimate [15] $E_C = 10 \text{ meV}$. In other implementations lowering the temperature of the device may be not that effective: comparing SAW- [17] and FET-based pumps [16] (traces “c” and “b” in Fig. 2 respectively), we see a large difference in δ_2 of the first plateaux. Despite a similarity in QD area, temperature and material implementation the maximally achievable accuracy according to our model is $\langle n - \langle n \rangle \rangle^2 \approx 10^{-3}$ for this particular SAW device versus 10^{-5} in the case

of the FET. Assuming that tunneling dominates in the latter case, δ_n is expected to scale proportional to the difference in localization lengths between the ground states with n and $n - 1$ charges.

In conclusion, we have proposed a scheme for accurate initialization of QDs and analyzed it quantitatively. We have shown that the model may be readily implemented using non-adiabatic pump architectures. It allows to extract a device-specific fingerprint which can be used to predict the results of a high precision measurement from a low precision characterization. In this way one can efficiently evaluate and optimize different pump architectures as required for fundamental metrology and adapt them for dynamic-QD-based quantum information devices.

We thank Ph. Mirovsky for discussions and T.J.B.M. Janssen for providing raw data for Fig. 2c. V.K. has been supported by ESF project No.2009/0216/1DP/1.1.1.2.0/09/APIA/VIAA/044. B.K. has been supported by EURAMET joint research project with European Community’s 7th Framework Programme, ERANET Plus under Grant Agreement No. 217257.

-
- [1] D. V. Averin and K. K. Likharev, *Mesoscopic Phenomena in Solids* (Elsevier, Amsterdam, 1991), pp. 173–271.
 - [2] D.Loss and D.P.DiVincenzo, *Phys.Rev.A* **57**, 120 (1998).
 - [3] J. M. Elzerman *et al.*, *Nature* **430**, 431 (2004).
 - [4] C. H. W. Barnes, J. M. Shilton, and A. M. Robinson, *Phys. Rev. B* **62**, 8410 (2000).
 - [5] G. Feve *et al.*, *Science* **316**, 1169 (2007).
 - [6] M. Kataoka *et al.*, *Phys. Rev. Lett.* **98**, 046801 (2007).
 - [7] T. Hayashi *et al.*, *Phys. Rev. Lett.* **91**, 226804 (2003).
 - [8] C.Liu and Q.Niu, *Phys.Rev.B* **47**, 13031 (1993).
 - [9] K. Flensberg, Q. Niu, and M. Pustilnik, *Phys. Rev. B* **60**, R16291 (1999).
 - [10] G. R. Aizin, G. Gumbs, and M. Pepper, *Phys. Rev. B* **58**, 10589 (1998).
 - [11] A. M. Robinson and C. H. W. Barnes, *Phys. Rev. B* **63**, 165418 (2001).
 - [12] M. D. Blumenthal *et al.*, *Nature Physics* **3**, 343 (2007).
 - [13] S. Miyamoto *et al.*, *Appl. Phys. Lett.* **93**, 222103 (2008).
 - [14] C. Leicht *et al.*, *Physica E*, doi:10.1016/j.physe.2009.11.109 (2009).
 - [15] A. Fujiwara, K. Nishiguchi, and Y. Ono, *Appl. Phys. Lett.* **92**, 042102 (2008).
 - [16] B. Kaestner *et al.*, *Appl. Phys. Lett.* **94**, 012106 (2009).
 - [17] J. T. Janssen and A. Hartland, *IEEE Trans. Instr. Meas.* **50**, 227 (2001).
 - [18] M. R. Astley *et al.*, *Phys. Rev. Lett.* **99**, 156802 (2007).
 - [19] B. Kaestner *et al.*, *Appl. Phys. Lett.* **92**, 192106 (2008).
 - [20] Y. M. Galperin, O. Entin-Wohlman, and Y. Levinson, *Phys. Rev. B* **63**, 153309 (2001).
 - [21] A. M. Robinson and V. I. Talyanskii, *Phys. Rev. Lett.* **95**, 247202 (2005).
 - [22] B. Kaestner *et al.*, *Phys. Rev. B* **77**, 153301 (2008).